Crystal Growth of Electronic Materials, edited by E. Kaldis

Chapter 12

CRYSTAL GROWTH AND ELECTRO-OPTIC PROPERTIES OF OXIDE SOLID SOLUTIONS

Hans J. SCHEEL

Institute of Physics and Chemistry of São Carlos, University of São Paulo, C.P. 369, 13.560 São Carlos SP, Brazil

and

Peter GÜNTER

Laboratory of Solid State Physics, Swiss Federal Institute of Technology, ETH-Hönggerberg, CH-8093 Zurich, Switzerland

Contents

1. Introduction

Oxide compounds of garnet-, perovskite-, spinel-, ilmenite-, distorted tungsten-bronze- and pyrochlore-type show a large variety of solid solutions. This is possible by the generally large anion to cation radius ratio, so that the cations with radii in the range 0.5 to 1.2 Å are replaceable within the oxygen lattice with the ionic radius of O^{2-} of 1.4 Å.

Pronounced solid solubility is found when the type of binding (ionic, covalent) is similar, when electroneutrality is achieved, and when the cation radii allows the same coordination number with oxygen, e.g. tetrahedral, octahedral etc. corresponding to coordination numbers 4, 6 etc. Solid solutions $A_{1-x}B_x$ allow one to optimize or to compromise the properties of the end members by adjustment of the free parameter x for magnetic, magneto-optic, piezoelectric and further applications.

Solid solutions also show phenomena which are not found in the end members as for instance hardening effects. In ferroelectric oxide solid solutions the ferroelectric phase transition with the anomaly in the dielectric constant can be adjusted with respect to the application (room) temperature so that the anomalously high electro-optical and birefringence effects can be used for numerous applications. In the next section the nonlinear-optic, electro-optic and photorefractive properties and applications are briefly discussed as examples of the potential of solid solutions. So far, however, this potential could not be used due to the unavailability of crystals of sufficient homogeneity, and the "striation problem" was regarded as an inherent or intrinsic problem of crystal growth [1–4].

The origin of inhomogeneity and specially of striations will be briefly reviewed in section three, together with the segregation problem and the relevant growth parameters. Specially, the role of hydrodynamics will be discussed, and the conventional approach of *reduced* convection will be con-

fronted with the proposed *forced* convection. In section four the results of systematic optimization of the growth parameters will be demonstrated with "striation-free" crystals of $KTa_{1-x}Nb_xO_3$ (KTN) solid solutions.

2. Electro-optic, nonlinear-optic and photorefractive properties

The electro-optic or nonlinear-optic effects may be defined as the dependence of the index of refraction (or the absorption coefficient) on dc or optical-frequency electric fields or lattice polarizations [5]. The field-induced changes of the refractive index n lead to the electro-optic Pockels and Kerr effects, the nonlinear-optic effect [5] and the photorefractive effect [6].

The electro-optical properties can be described in terms of field induced changes of the optical-index ellipsoid $\Delta(1/n^2)_{ij}$ by using the linear and quadratic electro-optic r and R coefficients, respectively, and the applied electric field E:

$$\Delta(1/n^2)_{ij} = r^{\mathrm{T}}_{ijk}E_k + R^{\mathrm{T}}_{ijkl}E_kE_l = (r^{\mathrm{S}}_{ijk} + p_{ijlm}d_{lmk})E_k + \cdots, \quad (1)$$

where T and S indicate constant stress and strain, and p_{ijlm} and d_{lmk} the photoelastic and piezoelectric tensors, respectively. The charge displacement within the crystal, the polarization P is related to the polarization-optic coefficients f_{ijl} and g_{ijkl} by

$$\Delta(1/n^2)_{ij} = f_{ijl}P_l + g_{ijkl}P_kP_l. \quad (2)$$

The linear electro-optic coefficients (EO) and polarization-optic coefficients (PO) are related by

$$r_{ijk} = f_{ijl}(\varepsilon_{lk} - \delta_{lk})\varepsilon_0, \quad (3)$$

with ε_{lk} being the dielectric tensor, ε_0 the free-space permittivity and δ_{lk} the Kronecker delta.

In ferroelectric materials based on oxygen-octahedra structures with the packing densities of octahedra $\xi = 1$ for perovskites, $\xi = 1.06$ for tungsten-bronze structures and $\xi = 1.21$ for $LiNbO_3$-type crystals [7], the birefringence in the polar phase can be defined in terms of the quadratic PO coefficients:

$$\Delta n = -\tfrac{1}{2}n_0^3\, g^0_{\mathrm{eff}}/\xi^3 P_s^2, \quad (4)$$

where n_0 is the refractive index of the unpolar materials, g^0_{eff} the temperature-independent quadratic PO coefficient, and P_s the spontaneous polarization. Thus, materials with high dielectric constant and spontaneous polarization and with large refractive index lead to large electro-optic effects. For electro-optic modulators of optical length l and electrode spacing z the voltage required for an optical retardation of half of the wavelength λ, the *half-wave voltage* V_π, is the relevant parameter:

$$V_\pi = \frac{\lambda}{n^3 r_c}\frac{z}{l} \simeq \frac{\lambda z \xi^3}{2\varepsilon_0 n^3 g^0_{\mathrm{eff}} l}\frac{1}{\varepsilon_{33} P_s}. \quad (5)$$

The product n^3r_c can be used as the figure of merit for electro-optic modulator applications, which is shown in fig. 1 with the optical transmission ranges for three solid-solution systems and for a few selected EO materials for comparison. The high efficiency of the solid solutions is due to the anomaly of the dielectric constant near the phase transitions. Accordingly the half-wave voltage is in a first approximation dependent only on the difference of the transition temperature T_c

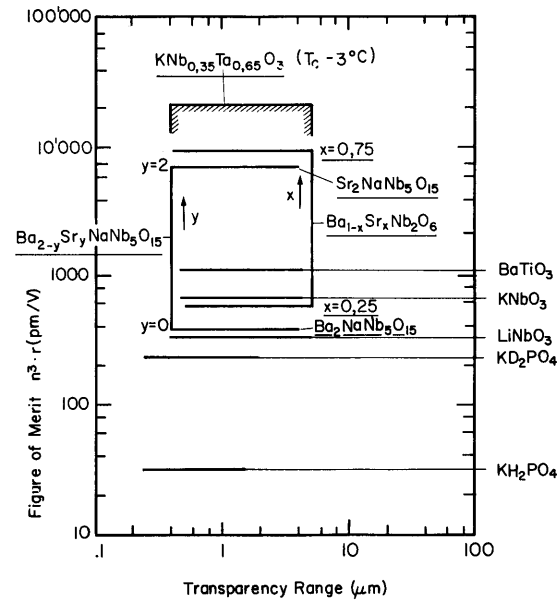

Fig. 1. Figures of merit and transparency ranges for electro-optic modulator materials including the solid solutions $KTa_{1-x}Nb_xO_3$, $Ba_{1-x}Sr_xNb_2O_6$ and $Ba_{2-y}Sr_yNaNb_5O_{15}$.

and the application (room) temperature, as is shown in fig. 2. Here the data are given for the electric fields applied parallel to the direction of spontaneous polarization for light with $\lambda = 633$ nm propagating perpendicular to the electric fields. However, the high EO efficiency and low half-wave voltage at $T_{appl} \approx T_c$ is partially offset by the high temperature sensitivity of the device [6, 12]. Thus the composition has to be chosen to compromise between the opposing requirements of high efficiency and low temperature sensitivity.

Further requirements for EO materials are a good optical homogeneity of the crystals, sufficient hardness and workability of the surfaces, low power requirement, small dielectric loss factor and small optically induced changes of refractive (or absorption) index, i.e. small light damage.

The optical homogeneity of the crystals should be high enough in order to assure that the optical length is within a fraction of a wavelength across the aperture of electro-optical devices. This in general requires $\Delta n \leq 10^{-6}$ over the illuminated area, i.e. crystals with small compositional fluctuations (striation-free crystals).

The main application of nonlinear-optic (NLO) effects is in producing coherent light in frequency ranges not available with laser sources, by sum-frequency — or difference-frequency — and second-harmonic generation (SHG) or optical rectification effects. For nonlinear-optical applications the *acentric* ABO_3-type materials with Ti–O, Nb–O, Ta–O and I–O bonds have the largest nonlinear bond polarizabilities in this order [8]. The requirements for NLO materials are high nonlinearity (piezoelectric materials with high refractive index), low sensitivity to optical damage, appropriate transmission range, phase-matching wavelength or angles, sufficient hardness and chemical stability, and of course an excellent optical perfection. The latter requirement may be specified by refractive-index variations (chemical homogeneity and strain birefringence) of less than 10^{-6} and by lack of scattering centers.

The SHG intensity is given by

$$I(2\omega) = \frac{2\omega^2 l^2}{c\varepsilon_0} \frac{d^2}{n^3} I^2(\omega) \left(\frac{\sin(\Delta k l/2)}{\Delta k l/2}\right)^2 \qquad (6)$$

for the ideal case of second-harmonic generation of plane monochromatic waves, neglecting pump depletion. Here l is the crystal length, c the vacuum velocity of light, d the nonlinear-optical coefficient, ω the light frequency of the fundamental wave with intensity $I(\omega)$, and $\Delta k = k_2 - 2k_1$ is the phase mismatch. The figures of merit for SHG generation (d^2/n^3) and the optical transmission

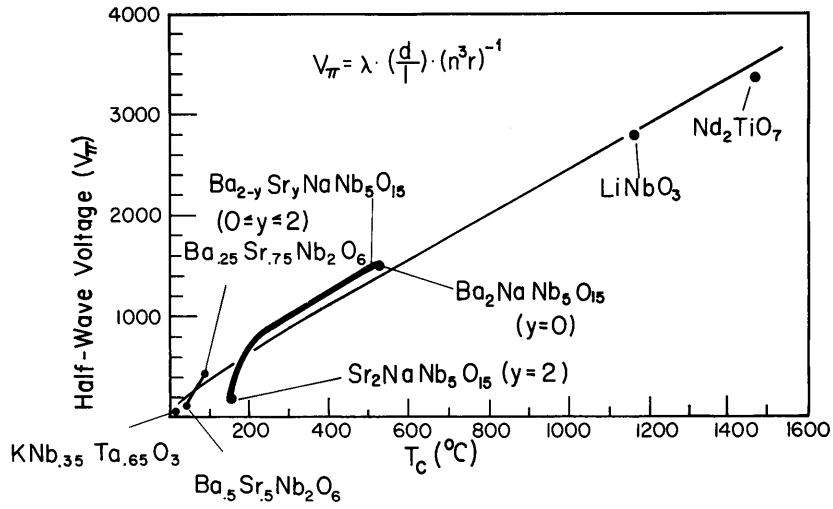

Fig. 2. Half-wave voltages versus T_c at $\lambda = 633$ nm for the solid-solution series $Ba_{2-y}Sr_yNaNb_5O_{15}$ (for $Ba_{0.5}Sr_{0.5}Nb_2O_6$ and $Ba_{0.25}Sr_{0.75}Nb_2O_6$ and for $KTa_{0.65}Nb_{0.35}O_3$) and for $LiNbO_3$ and $Nd_2Ti_2O_7$ for comparison.

ranges for the solid solution system $Sr_{1-x}Ba_xNb_2O_6$, for $Ba_2NaNb_5O_{15}$ and for other materials for comparison are shown in fig. 3. In these materials the transmission range includes the visible region. There are NLO materials with transmission ranges in the infrared like $AgGaSe_2$, $ZnGeP_2$ and Te which have much higher figures of merit due to very large NLO coefficients and high refractive indices. Lately organic crystals and polymers have been found with very large nonlinearities and optical damage thresholds [9, 10] which thus may compete with the oxide solid solutions for applications where hardness and surface workability are of minor importance.

New fields of applications of oxide solid solutions are in signal processing (holographic storage, page composers, optical bistable elements, components producing waves with complex conjugate amplitudes with respect to a given wave amplitude etc.). These applications are based on suitable photorefractive [6], electro-optical or nonlinear-optical materials [11]. Photorefractive materials with large photo-induced refractive-index changes at relatively low light power are of great interest for "real-time" optical signal processing [11]. The index changes are caused by photo-induced space-charge fields. The main material requirements are large electro-optic r coefficients, an excitation-trapping mechanism for photo-excited carriers, and an efficient transport for these carriers [11].

In oxygen-octahedra ferroelectrics, impurities like Fe, Mn, Ce, Cu, Ni, U, Mo etc. are responsible for photo-excitation and trapping. Oxide solid solutions with high packing densities $\xi > 1$, e.g. the tungsten-bronzes, offer doping sites with coordination numbers 6, 9, or 12. Transport of photo-excited carriers is provided by the bulk photovoltaic effect, diffusion, or by photoconductivity (drift in an applied external field) [11]. The latter mechanism is preferred for "real-time" recording.

In a first approximation the recording time of illuminated dielectric layers is

$$t = \frac{h\nu}{e} \frac{\varepsilon\varepsilon_0}{\Phi\alpha I} \frac{1}{\mu\tau}, \tag{7}$$

where $h\nu$ is the photon energy, e the electron charge, Φ the quantum efficiency for exciting a unit charge carrier, α the absorption coefficient, I the light intensity, μ the mobility and τ the lifetime of excited carriers. In oxygen-octahedra dielectrics $t = 1$ ms requires $0.1\ \mu s < \tau < 1\ \mu s$. At a given intensity the recording time is defined

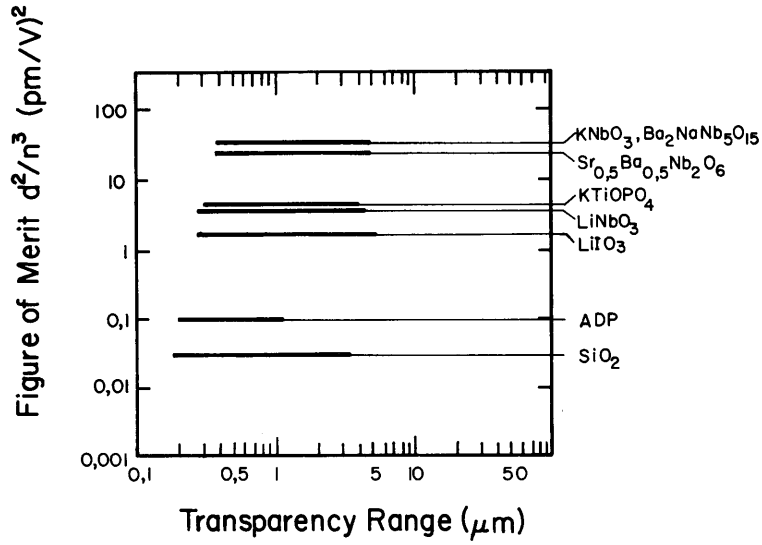

Fig. 3. Figures of merit and transparency ranges for the solid-solution $Sr_{1-x}Ba_xNb_2O_6$, for $Ba_2NaNb_5O_{15}$ and for other NLO materials.

primarily by the carrier lifetime which depends on the concentration ratio of donors to traps. This ratio can be adjusted by oxidation–reduction treatment during or after crystal growth, for instance for the impurity Fe by the reversible reaction

$$2Fe^{3+} + O^{2-} \underset{\text{oxidation}}{\overset{\text{reduction}}{\rightleftarrows}} 2Fe^{2+} + \tfrac{1}{2}O_2,$$

where Fe^{2+} act as donors and Fe^{3+} as acceptors. Charge compensation in the reduction treatment is achieved by the formation of oxygen vacancies.

The maximum refractive index change by the electro-optic effect is

$$\Delta n_{max} = \tfrac{1}{2} n^3 r_{eff} E_{SC}, \tag{8}$$

where E_{SC} is the photo-induced space-charge field (which mainly depends on the trapping center concentration). Experiments show that the index change is in the range $10^{-5} < \Delta n < 10^{-3}$ in most of the photorefractive materials. Table 1 shows data for $\mu\tau$, $t_1 = t(\Phi\alpha I = 1\ \text{W/cm}^2)$ and r_{max} for the photoconductive oxide solid solutions $Ba_{0.25}Sr_{0.75}Nb_2O_6$ and $KTa_{0.65}Nb_{0.35}O_3$ ($T_c = 40°C$) and for other photorefractive materials for comparison.

3. Inhomogeneities and growth parameters

Inhomogeneities in doped crystals or in solid solutions may have various origins: (a) macrosegregation leading to bulk concentration gradients, (b) growth-rate fluctuations leading to striations, (c) locally differing growth mechanisms and growth rates leading to striation-like inhomogeneities, and (d) instability-induced growth-rate fluctuations and striations. The latter two causes of inhomogeneities can be reduced or eliminated by achieving a single growth mechanism on either an atomically flat surface with propagating microsteps [13], or on a rough surface (c), and by growing the crystal in a stable growth regime in order to prevent the instability-induced fluctuations [14].

The major homogeneity problems, macrosegregation and the *striation-problem*, are schematically indicated in fig. 4 with the phase diagram of the solid-solution system $KTaO_3$–$KNbO_3$ [15]. If crystals are grown by the slow-cooling technique by reduction of the temperature from T_1 to T_2, the Nb concentration in the crystal will change from x_1 to x_2. This *Inherent Concentration Gradient* (ICG) can be reduced by using large melt to crystal ratios [16] (and thus small growth temperature intervals) and by optimized cuts of the samples. A conventional approach to reduce the ICG are transport techniques where feed materials are dissolved at the higher temperature T_3 and transported to the growing crystal at T_4 [17, 18].

Whereas the ICG can be eliminated, the temperature differences ($T_3 - T_4$) required to achieve a reasonable growth rate so far lead to striations, even when forced convection is applied. If crystals for electro-optic, photorefractive, or nonlinear-

Table 1
Photoconductivity parameter $\mu\tau$, recording time t and electro-optic coefficient for photo-refractive materials (from ref. [6]).

Material	Photoconductivity $\mu\tau(10^{-11}$ m/V)	Recording time $t(\phi\alpha I = 1\ \text{W/cm}^2)$ (ms)	Electro-optic coefficient r_{ij} (pm/V)
$Bi_{12}SiO_{20}$	1	0.2	5
$Bi_{12}GeO_{20}$	0.8	0.2	3.4
$LiNbO_3$	0.01	30 000	31
$BaTiO_3$	0.001	40	60, 1600
$KNbO_3 : Fe^{2+}$	0.3	0.5	64, 380 (r_{42})
K(Nb, Ta)O_3 ($T_c = 40°C$)	0.01	(10)	~500
$Ba_{0.25}Sr_{0.75}Nb_2O_6$	0.8	0.5	45

optical applications are to be grown the inhomogeneity should be smaller than 10^{-6} for Δn, i.e., ΔT_c should be within 0.02°C. The corresponding composition homogeneity Δx should then be smaller than 0.000 03. With the slope of the solidus curve this corresponds to a temperature stability requirement at the growth interface of less than 0.01°C. As this could not be achieved at high growth temperatures, the striation-problem could not be solved. Only very recently striations could be eliminated by applying the slow-cooling technique in combination with high-precision temperature control and forced convection. Before these results are presented in section 4, the role of hydrodynamics on crystal homogeneity should be clarified.

Striations have long been related to oscillatory convection and related temperature fluctuations [19, 20]. Therefore the general approach has been to reduce convection in order to reduce striations, for instance by reduction of the melt height, by magnetic damping and by experiments in reduced gravity (Skylab, Spacelab). The role of convection can be recognized with the Burton–Prim–Slichter [21] (BPS) segregation analysis. Since in growth of homogeneous crystals the experimentalist tries hard to achieve steady-state growth conditions, the steady-state approximations of BPS for growth from melts and of Van Erk [22] for growth from diluted solutions may be applied.

The BPS equation

$$k_{\text{eff}} = \frac{k^*}{k^* + (1 - k^*)\exp(-v\delta/D)} \tag{9}$$

relates the effective distribution coefficient k_{eff} to the interface distribution coefficient k^*, the growth rate v, the diffusion boundary layer thickness δ and the diffusion coefficient D. In most cases the interface distribution coefficient (concentration ratio of the solid to that in the liquid at the solid–liquid interface), or the supersaturations are not precisely known. Since in case of stirred concentrated solutions or melts the interface concentration is practically identical with the concentration in the bulk of the solution, k^* in the BPS equation can be replaced by the equilibrium distribution coefficient $k_0 = C_S/C_L$ (concentration ratio of the solid to that in the bulk liquid

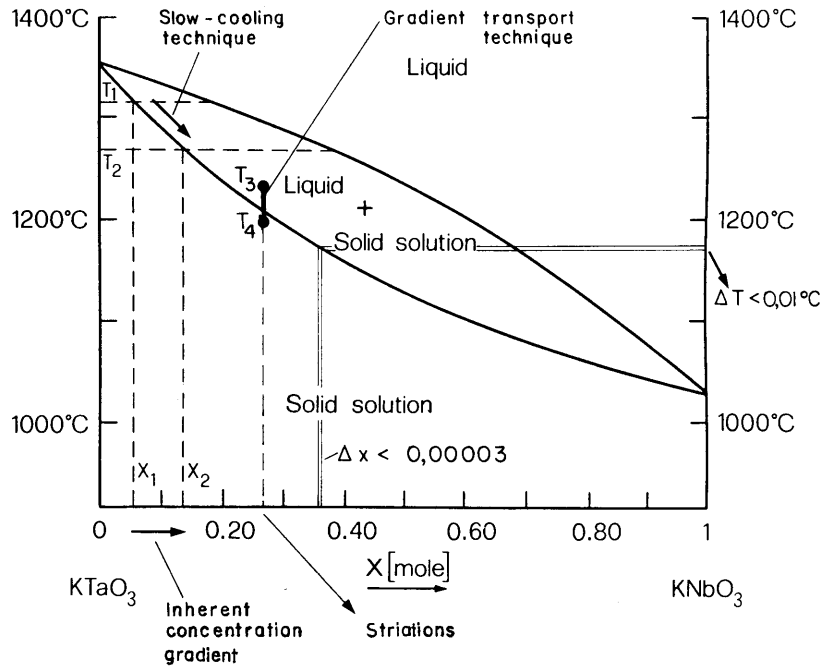

Fig. 4. Phase diagram of $KTa_{1-x}Nb_xO_3$ with indicated growth techniques and resulting inhomogeneities.

which can be simply derived from phase equilibria data).

Depending on whether volume diffusion, heat flux, or interface kinetics are the rate-limiting step, a correction of eq. (9) may be necessary for the interface relations as discussed by BPS [21], Trainor and Bartlett [23] and by Van Erk [22].

For incomplete mixing the growth rate is inversely proportional to the diffusion boundary layer thickness, so that the exponent in the BPS equation remains unaffected (k_0 and D can be regarded constant in this case). Thus, hydrodynamic changes are compensated by corresponding growth-rate changes, whereas growth-rate changes caused by temperature fluctuations are not compensated and thus lead to changes of k_{eff} and therefore to striations [24, 25]. The consequence of the foregoing is that hydrodynamic fluctuations by themselves do not induce striations; only temperature fluctuations at the interface (for instance by convective transport of liquid of varying temperature towards the interface) are responsible for striations. Therefore, the reciprocating stirring in crystallization from aqueous solutions and the accelerated crucible rotation technique (ACRT) [26, 17] for growth from high-temperature solutions are suitable for growth of homogeneous crystals as long as the system is isothermal, at least at the growth interface.

Forced convection has other advantages as it helps to homogenize the melts or solutions; it thus facilitates nucleation control, material transport and heat transfer to and from the growth interface and the apparatus is relatively simple (stirrer or ACRT). Problematic is the application of forced convection to Czochralski growth, although the parabolic deformation of the liquid surface can be compensated by synchronized crucible or crystal height corrections [27].

Reduced convection, on the other hand, is either not easily achieved by simple means (e.g. shallow melts), or requires large efforts with a magnetic damping field or with reduced gravity. Other problems of reduced convection are low efficiency of material transport towards the growing interface, or homogeneization of melt or solution. Therefore, forced convection should be applied in crystal growth processes whenever possible [26, 24].

4. Optimized growth conditions and results

The results of growing crystals of $KTa_{1-x}Nb_xO_3$ solid-solutions (a) with $x < 0.04$ [16] and (b) with $x \approx 0.26$ [28] have been published recently and therefore will be discussed only briefly here. The KTN crystals have been grown by the slow-cooling technique from melts containing excess K_2CO_3. The latter decomposes, giving off CO_2, and thus the solvent consists of $K_3Ta_{1-y}Nb_yO_4$ [16]. The solution was homogenized by the accelerated crucible rotation technique ACRT during the dissolution phase as well as during the growth run; this also allowed control of the nucleation and increased maximum stable growth rates. Typical ACRT data are 60 to 90 rpm with periods between 60 and 120 s for the soaking period, and 30 to 60 rpm with periods between 40 and 120 s for the growth phase. Spontaneous nucleation occurred during slow cooling, and the number of nuclei was reduced by temperature oscillation in the initial phase. Then the temperature was reduced at a rate between 0.13 and 0.18°C per hour for the slow-cooling experiments, whereas for the temperature-gradient experiments the thermal gradients were not known exactly and assumed to be more than 1°C cm^{-1} in the melt. Since the KTN crystals grown by gradient transport showed defined striations (see fig. 5) with a periodicity corresponding to ACRT periodicity and growth rate, the slow-cooling technique and a nearly isothermal arrangement of the crucible were applied to reduce striations.

As discussed in the preceding section, a very critical parameter is the temperature control. By using a sixfold thermopile of PtRh6% versus PtRh30% thermocouples [29], a high sensitivity at high temperatures (63 μV/°C) and a low sensitivity of the cold junctions at room temperature (< 0.4 μV/°C) can be achieved.

This temperature sensor in combination with commercial high-quality PID controllers and programmers (Eurotherm) and with optimized design of the control and measurement systems allows a precision of temperature control with a standard deviation of 0.03°C and maximum deviations from the ideal program of 0.075°C [17, 28]. Due to the large thermal mass of the platinum crucible and the ACRT-homogenized melt within

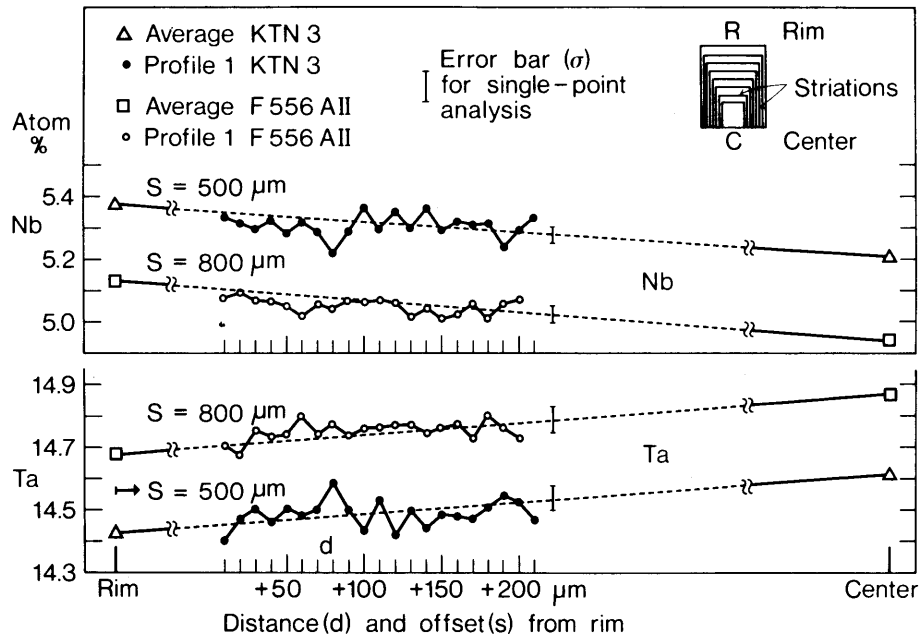

Fig. 5. Electron microprobe analyses [27] of KTN crystals ($x \approx 0.26$) grown by gradient transport (sample KTN3) and by slow-cooling technique (F556AII).

the nearly isothermal furnace, one can expect the temperature fluctuations at the growth interface to be less than the required 0.01°C shown in fig. 4.

The resulting crystals of sizes between 5 mm and 35 mm and weights up to 114 g were striated when grown by gradient transport. Although the striations could clearly be recognized in a polarizing microscope, the electron microprobe analysis [28] revealed very small fluctuations in the Nb and Ta content only, even with counting times of 40 s per point. However, the Nb and Ta fluctuations of this sample KTN3 are correlated as can be recognized in fig. 5.

For the sample F556AII, which had been grown by the slow-cooling technique in quasi isothermal environment, no correlation of the Nb and Ta analyses can be recognized. Since this crystal does not show striations by the strain birefringence test in polarized light, it can be regarded as "striation-free". Also by interferometry striations could not be detected. If striations were present, they would have to be smaller than 1 μm, or the concentration fluctuations would lie below the detection limit of the electron microprobe.

5. Discussion

Solid solutions of oxide compounds of perovskite-, tungsten-bronze- and pyrochlore-type are of special interest for numerous applications due to the large electro-optic and nonlinear-optic coefficients, high refractive indices etc. As the severe requirements of optical homogeneity could not be solved by crystal growers, the applications of solid solutions were rather limited so far.

The present analysis of the inhomogeneity problem, especially of the striation problem, has shown that hydrodynamic fluctuations themselves are only weekly responsible, if at all, for striations. In most cases the striations are caused by temperature fluctuations at the interface which generally are correlated with convective oscillations.

The general approach to the striation problem, therefore, was to reduce convection with the disadvantages of restricted mass transport and large required efforts (magnetic fields, Spacelab). As was shown in sections 3 and 4, a more efficient approach to solve the striation problem is smooth

forced convection which, in combination with excellent temperature control and sufficiently small temperature gradients, allowed the growth of "striation-free" KTN crystals for the first time. These crystals have been grown from highly concentrated high-temperature solutions. Further experimental and theoretical work is necessary to show whether smooth forced convection helps to reduce or to eliminate striations also in Czochralski-grown crystals.

References

[1] H. Fay, Mater Res. Bull. 2 (1967) 499.
[2] R.L. Byer, Ann. Rev. Mat. Sci. 4 (1974) 147.
[3] A. Räuber, in: Current Topics in Materials Science 1 (1978) 481.
[4] P. Reiche, R. Schalge, J. Bohm, D. Schultze, Kristall und Technik 15 (1980) 23.
[5] S.H. Wemple and M. DiDomenico, in: Applied Solid State Science, Vol. 3, ed. R. Wolfe (Academic Press, New York, 1972) p. 264.
[6] P. Günter, Phys. Rep. 93 No. 4 (1982) 199.
[7] S.H. Wemple and M. DiDomenico, J. Appl. Phys. 40 (1969) 720, 735.
[8] J.G. Bergman and G.R. Crane, J. Solid State Chem. 12 (1975) 172.
[9] J. Zyss, J. Non-Cryst. Solids 47 (1982) 211.
[10] A.F. Garito and K.D. Singer, Laser Focus (Feb. 1982) p. 59.
[11] P. Günter, Dielectric materials for optoelectronic devices, in: Proc. Journées d'Electronique '82 (Press Polytechniques Romandes, Lausanne, 1982) p. 15.
[12] P. Günter, Ferroelectrics 24 (1980) 35.
[13] H.J. Scheel, Appl. Phys. Lett. 37 (1980) 70.
[14] A.I. Landau, Phys. Met. Metallogr. 6 (1958) 148.
[15] A. Reisman, S. Triebwasser and F. Holtzberg, J. Am. Chem. Soc. 77 (1955) 4228.
[16] D. Rytz and H.J. Scheel, J. Cryst. Growth 59 (1982) 468.
[17] D. Elwell and H.J. Scheel, Crystal Growth from High-Temperature Solutions (Academic Press, London, New York, 1975) Ch. 7.
[18] W. Tolksdorf and F. Welz, J. Cryst. Growth 20 (1973) 47.
[19] A. Müller and M. Wilhelm, Z. Naturforsch. 19a (1964) 254.
[20] D.T.J. Hurle, Phil. Mag. 13 (1966) 305.
[21] J.A. Burton, R.C. Prim and W.P. Slichter, J. Chem. Phys. 21 (1953) 1987.
[22] W. Van Erk, J. Cryst. Growth 57 (1982) 71.
[23] A. Trainor and B.E. Bartlett, Solid State Electron. 2 (1961) 106.
[24] H.J. Scheel and E.O. Schulz-DuBois, in: Convective Transport and Instability Phenomena (Braun, Karlsruhe, 1982) p. 491.
[25] H.J. Scheel and R.H. Swendsen, in preparation.
[26] H.J. Scheel, J. Cryst. Growth 13/14 (1972) 560; H.J. Scheel and E.O. Schulz-DuBois, J. Cryst. Growth 8 (1971) 304.
[27] H.J. Scheel and H. Müller-Krumbhaar, J. Cryst. Growth 49 (1980) 291.
[28] H.J. Scheel and J. Sommerauer, J. Cryst. Growth 62 (1983) 291.
[29] H.J. Scheel and C.H. West, J. Phys. E 6 (1973) 1178.